Astronomy
&
Astrophysics

Hα surface photometry of galaxies in nearby clusters

V. The survey completion[*],[**]

G. Gavazzi[1], A. Boselli[2], L. Cortese[1,2], I. Arosio[1], A. Gallazzi[3], P. Pedotti[1], and L. Carrasco[4]

[1] Università degli Studi di Milano-Bicocca, Piazza delle scienze 3, 20126 Milano, Italy
   e-mail: giuseppe.gavazzi@mib.infn.it
[2] Laboratoire d'Astrophysique de Marseille, BP8, Traverse du Siphon, 13376 Marseille Cedex 12, France
[3] Max-Planck-Institut für Astrophysik, Karl-Schwarzschild-Str. 1, 85748 Garching bei München, Germany
[4] Instituto Nacional de Astrofísica, Optica y Electrónica, Apartado Postal 51. CP 72000 Puebla, Pue., México

ABSTRACT

We present the Hα imaging observations of 273 late-type galaxies in the nearby rich galaxy clusters Virgo, A 1367, Coma, Cancer, Hercules and in the Great Wall, carried out primarily with the 2.1 m telescope of the San Pedro Martir Observatory (SPM) and with the ESO/3.6 m telescope. We derived the Hα+[NII] fluxes and equivalent widths. The Hα survey reached completion for an optically selected sample of nearby galaxies in and outside rich clusters. Taking advantage of the completeness of the data set, the dependence of Hα properties on the Hubble type was determined for late-type galaxies in the Virgo cluster. Differences in the gaseous content partly account for the large scatter of the Hα *EW* within each Hubble-type class. We studied the radial distributions of the Hα *EW* around Coma+A 1367 and the Virgo clusters in two luminosity bins. Luminous galaxies show a decrease in their average Hα *EW* in the inner ~1 virial radius, while low-luminosity galaxies do not show this trend.

Key words. galaxies: photometry – galaxies: clusters: individual: Virgo, Coma, A 1367, Cancer

1. Introduction

The Hα emission arising from HII regions is the most direct indicator of the current ($<4 \times 10^6$ yrs), massive (>8 $M_\odot$) star-formation activity in galaxies (Kennicutt 1998). Extensive Hα imaging surveys of galaxies are being undertaken by several investigators, among others: Almoznino & Brosch (1998); Moss & Whittle (2000); Sakai et al. (2001); Koopmann et al. (2001); James et al. (2004). On our part we undertook an Hα observing campaign of galaxies in nearby clusters and superclusters that originated in 1990 using the aperture photometer at the KPNO 1.3 m telescope (Gavazzi et al. 1991). As soon as imaging capabilities were offered by panoramic detectors, it continued with the use of various other facilities. A generous time allocation was obtained at the San Pedro Martir 2.1 m telescope, allowing us to observe galaxies in the Cancer cluster and in the two clusters (Coma and A 1367) in the Great Wall

(Gavazzi et al. 1998). Taking advantage of the large field of view offered by the WFC at the INT, a 1 sq deg. region of each of these clusters was fully imaged (Iglesias-Paramo et al. 2002). Later on we focused on the Virgo cluster, again making extensive use of the SPM telescope (Gavazzi et al. 2002a, Paper I of this series; 2002b, Paper IV), of the 1.2 m OHP and Calar Alto telescopes (Boselli & Gavazzi 2002, Paper II) and of the 2 m INT and NOT telescopes (Boselli et al. 2002, Paper III).

The present set of 273 Hα observations of fainter targets, as described in Sect. 2, represents the near completion of the Hα survey of late-type members of the Virgo cluster down to 18.0 mag and of members of the Coma supercluster and of the Cancer cluster down to the limiting magnitude of 15.7. All products of the present Hα survey, including images, are available worldwide from the site GOLDmine (http://goldmine.mib.infn.it/) (Gavazzi et al. 2003).

A forthcoming paper of this series (Paper VI, in preparation) will analyze the full Hα data-set in conjunction with other parameters from GOLDmine, e.g. the HI properties, with the aim of deriving the radial distribution of the star-forming regions as a function of the gaseous properties of galaxies in and outside rich clusters.

---

[*] Based on observations taken at the observatory of San Pedro Martir (Baja California, Mexico) of the Observatorio Astronómico Nacional (OAN), Universitad Autonoma de Mexico (UNAM).

[**] Tables 1 and 2 are only available in electronic form at the CDS via anonymous ftp to cdsarc.u-strasbg.fr (130.79.128.5) or via http://cdsweb.u-strasbg.fr/cgi-bin/qcat?J/A+A/446/839

2. The new data

2.1. Selection criteria

Observations of 273 galaxies were obtained in the Virgo and Cancer clusters in the Coma/A 1367 and Hercules superclusters according to the following selection criteria:

- their Hubble type is Sa or later (Sa-Im-BCD).
- they have a measured redshift.
- *Virgo cluster*: they are brighter than $m_{pg} = 18.0$ mag in the Virgo Cluster Catalogue (VCC) of Binggeli et al. (1985); they are classified as members of cluster A or B, as possible members or belonging to the W, W′, M clouds or to the southern extension (Binggeli et al. 1985, 1993; Gavazzi et al. 1999a); their redshift is $V < 3000$ km s^{-1}; 127 Virgo galaxies matching these selection criteria were observed in this work.
- *Coma/A 1367 supercluster*: they are brighter than $m_{pg} = 15.7$ mag in the CGCG (Zwicky et al. 1961–68); they are members of the Coma (A1656) or A 1367 clusters (C) to groups (G), multiplets (M) or they are isolated members (I) of the Great Wall ($4000 < V < 10\,000$ km s^{-1}) according to Gavazzi et al. (1999b); 104 galaxies matching these criteria are reported.
- *Cancer cluster*: they are brighter than $m_{pg} = 15.7$ mag in the CGCG (Zwicky et al. 1961–68) and are members of any of the subunits constituting the Cancer cluster according to Bothun et al. (1983); 33 galaxies matching these criteria are reported.
- *Hercules supercluster*: they are brighter than $m_{pg} = 15.7$ mag in the CGCG (Zwicky et al. 1961–68) and belong to either A2147 or A2151 or A2197 or A2199; 9 galaxies matching these criteria were observed as fillers.

The 273 target galaxies are listed in Table 1 as follows:

- Col. 1: VCC/CGCG designation, from Binggeli et al. (1985) for Virgo, or from Zwicky et al. (1961–68) for the Coma supercluster, Cancer and Hercules;
- Col. 2: NGC/IC name;
- Col. 3: UGC name (Nilson 1973);
- Cols. 4 and 5: J2000 celestial coordinates from GOLDmine;
- Cols. 6 and 7: major and minor optical diameters (arcmin). We measured for VCC galaxies the diameters on the du Pont plates at the faintest detectable isophote, as listed in the VCC. For CGCG galaxies, these are the major and minor optical diameters (a_{25}, b_{25}) that were derived, as explained in Gavazzi & Boselli (1996);
- Col. 8: heliocentric velocity (km s^{-1}) from the VCC or from Gavazzi et al. (1999a,b) or from NED;
- Col. 9: membership in a cluster or supercluster, defined as in Gavazzi et al. (1999a) for Virgo and in Gavazzi et al. (1999b) for the Coma/A 1367 supercluster;
- Col. 10: the distance (Mpc); we assumed 17 Mpc for Virgo cluster A and the distances given in Gavazzi et al. (1999a) for the various substructures of Virgo, 96 Mpc for galaxies in Coma and 91 Mpc for A 1367. Cancer galaxies were assigned to individual groups, each with a mean distance.
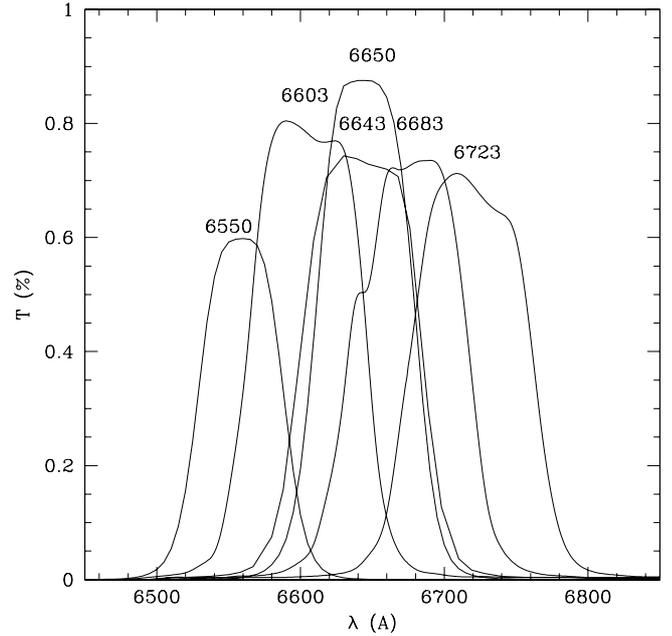

Fig. 1. The transmission profiles of the adopted narrow-band filters.

For galaxies not belonging to the clusters, the distance was determined from the individual redshifts, assuming $H_0 = 75$ km s^{-1} Mpc^{-1};
- Col. 11: morphological type as given in the VCC or in Gavazzi & Boselli (1996);
- Col. 12: photographic magnitude, as given in the VCC or in the CGCG;
- Col. 13: total B magnitude determined and corrected for Galactic (according to Burstein & Heiles 1978) and for internal extinction, as described in Boselli et al. (2003).

2.2. Observations

Narrow-band imaging in the Hα emission line ($\lambda = 6562.8$ Å) of 273 galaxies listed in Table 1 was obtained during 20 nights distributed in 3 runs: 2003 (Feb. 26–28), 2004 (Mar. 10–16) and 2005 (Apr. 9–17) using the 2.1 m telescope at San Pedro Martir Observatory (Baja California, Mexico). Another 18 galaxies with velocity <350 km s^{-1} that could not be observed at SPM, due to the lack of appropriate filters, were observed in 2005 (three half-nights; Mar. 14–16) using EFOSCII attached to the ESO/3.6 m telescope (proposal 074.B-0004).

The ($f/7.5$) SPM Cassegrain focus was equipped with an SIT3 1024×1024 pixels CCD detector with a pixel size of 0.31 arcsec. Each galaxy was observed through a narrow band (~90 Å) interferometric filter centered at the redshifted wavelength of the Hα line, including the side [NII] lines. Four filters of similar characteristics were used: λ 6603, 6643, 6683, 6723 Å, covering $350 < V < 9000$ km s^{-1} (see Fig. 1). The stellar continuum subtraction was secured by means of shorter observations taken through a broad-band r (Gunn) filter (OFF-band frame). The typical integration time was 15–30 min for the ON-band, sometimes split into shorter exposures, and 4 min for the OFF-band frame. The observations were mostly obtained in photometric conditions, with the seeing ranging
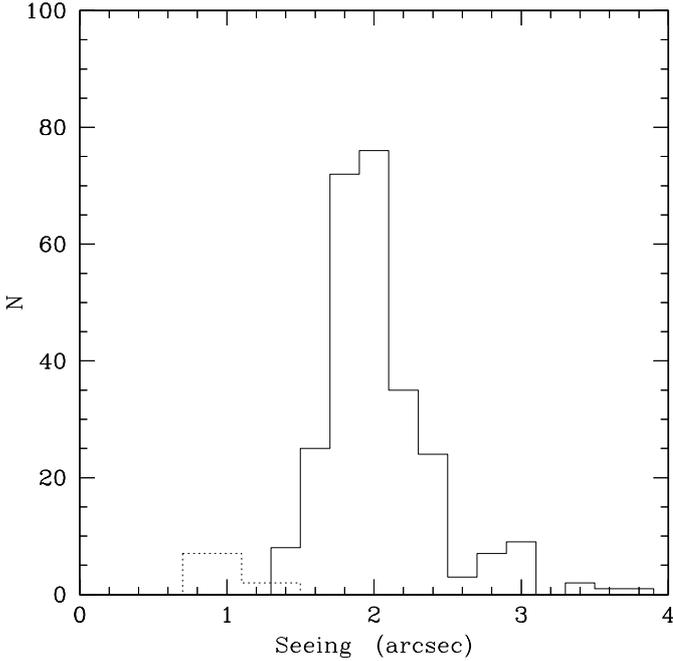
Fig. 2. The seeing distribution in the ON-band frames, separately for ESO (dotted) and SPM (continuous).

from 1.5 to 3 arcsec (see Fig. 2). The observations were flux-calibrated using the standard stars Feige 34 and Hz44 from the catalog of Massey et al. (1988), observed every 2–3 h. Periods with thin clouds were devoted to targets that were already observed with aperture photometers providing the zero point.

The ESO/3.6 m telescope was equipped with EFOSCII, 2048 × 2048 pixels LORAL detector used in the ×2 rebin mode with an effective scale of 0.314 arcsec per pixel. Two filters of ~80 Å width, centered at λ 6550 and 6650 Å, provided the ON-band frames (see Fig. 1) and the stellar continuum was taken through the r (Gunn) filter. The observations were obtained in photometric conditions, with the seeing ranging from 0.8 to 1.2 arcsec (see Fig. 2). The observations were flux-calibrated using the standard stars LTT3864 and LTT6248 from Hamuy et al. (1994) observed every 2–3 h. Repeated measurements of standard stars obtained at either ESO or SPM in photometric conditions gave <0.05 mag differences, so that we assumed that the typical uncertainty (1σ) of the photometric results given in this work was within 5%.

2.3. Data reduction

The reduction of the CCD frames followed a procedure that was identical to the one described in previous papers (e.g. Gavazzi et al. 2002b), based on the IRAF STSDAS[1]

---

[1] IRAF is the Image Analysis and Reduction Facility made available to the astronomical community by the National Optical Astronomy Observatories, which are operated by AURA, Inc., under contract with the US National Science Foundation. STSDAS is distributed by the Space Telescope Science Institute, which is operated by the Association of Universities for Research in Astronomy (AURA), Inc., under NASA contract NAS 5–26555.

reduction packages, which is briefly summarized here. To remove the detector response, each image was bias subtracted and divided by the median of several flat-field exposures obtained on empty regions of the twilight sky. When three images in the same filter were available, a median combination of the realigned images allowed removal of cosmic rays. For galaxies observed in single exposures, cosmic ray removal, as well as subtraction of contaminating objects, such as nearby stars and galaxies, was obtained by direct inspection of the frames. The sky background was determined in each frame in concentric object-free annuli around the object and then subtracted from the flat-fielded image. The typical uncertainty on the mean background was estimated to be 10% of the rms in the individual pixels. This represents the dominant source of error in low S/N regions.

2.4. The measured Hα+[NII] parameters

The flux from the [NII] emission lines (λ 6548-6584 Å) bracketing Hα was included in the ON-band observations. Hereafter we use the simplified notation "Hα" to refer to "Hα+[NII]". Both the flux and the EW of the Hα line can be recovered from narrow ON-band observations by subtracting the continuum contribution estimated using broad-band (r) images, once these are normalized to account for the ratio of the transmissivity of the two filters. The normalization coefficient n can be derived by assuming that field stars (with null Hα in emission) have identical flux in the ON- and OFF-band frames. By integrating the counts over diaphragms containing the studied galaxies in the ON and OFF frames, the net counts are given by:
$$C_{\text{NET}} = C_{\text{ON}} - nC_{\text{OFF}}.$$
The net flux in the Hα line is given by

$$F(\text{H}\alpha)_0 = Zp \frac{C_{\text{NET}}}{TR_{\text{ON}}(6563 \times (1+z))}, \tag{1}$$

and the equivalent width by

$$\text{H}\alpha\,EW_0 = \frac{\int R_{\text{ON}}(\lambda)\mathrm{d}\lambda}{R_{\text{ON}}(6563 \times (1+z))} \frac{C_{\text{NET}}}{nC_{\text{OFF}}}. \tag{2}$$

A non-negligeable (~10 percent) correction accounts for the contamination of the Hα line emission in the broad band filter (OFF-band) according to (see Paper III)

$$F(\text{H}\alpha) = F(\text{H}\alpha)_0 \left(1 + \frac{\int R_{\text{ON}}(\lambda)\mathrm{d}\lambda}{\int R_{\text{OFF}}(\lambda)\mathrm{d}\lambda}\right) \tag{3}$$

and

$$\text{H}\alpha EW = \text{H}\alpha EW_0 \left(1 + \frac{\text{H}\alpha EW_0}{\int R_{\text{OFF}}}\right)\left(1 + \frac{\int R_{\text{ON}}(\lambda)\mathrm{d}\lambda}{\int R_{\text{OFF}}(\lambda)\mathrm{d}\lambda}\right), \tag{4}$$

where T is the integration time (s), z the galaxy redshift and Zp the ON-band zero point (erg cm^{-2} s^{-1}) corrected for atmospheric extinction. $R_{\text{ON}}(\lambda)$ and $R_{\text{OFF}}(\lambda)$ are the transmissivities of the ON and OFF filters, respectively. The errors on these parameters are determined using Eqs. (6) and (7) from Paper I. The results of the present observations are listed in Table 2 as

follows:

- Col. 1: galaxy designation;
- Col. 2: year of the observation;
- Col. 3: Telescope;
- Col. 4: ON-band filter;
- Col. 5: transmissivity R_{ON} of the ON-band filter at the red-shifted Hα line;
- Col. 6: normalization factor n of the OFF-band frame;
- Col. 7: number of combined exposures times the integration times (T_{ON};) (in seconds) of the individual ON band exposures;
- Col. 8: photometric Zero point (Zp), such that $\mathrm{Log}Flux = Zp + \mathrm{Log}C_{NET} - \mathrm{Log}T_{ON}$ [erg cm^{-2} s^{-1}];
- Col. 9: flag indicating whether the frame was taken under photometric (P) or through light cirrus (C);
- Col. 10: HαEW with error, in Å as determined from this work;
- Col. 11: Logarithm of the Hα flux, in erg cm^{-2} s^{-1} as determined from this work;
- Cols. 12 and 13 and 14: HαEW and flux from the literature, with references.

All Hα and OFF-band images of galaxies observed in this work can be obtained in the FITS format from `http://goldmine.mib.infn.it/` (Gavazzi et al. 2003).

2.5. Comparison with the literature

Among the 56 galaxies measured in this work that have independent measurements in the literature (see Table 2), we selected those observed in photometric conditions. The two sets of measurements are in satisfactory agreement, as illustrated in Figs. 3 and 4. The linear regression between our equivalent width and flux measurements and those found in the literature are:

HαEW_{TW} = 0.84 × HαEW_L + 4.44
and
$\log F(Hα)_{TW} = 1.03 \times \log F(Hα)_L + 0.36$.

Literature measurements taken with aperture photometers (crosses in Figs. 3 and 4) show larger discrepancies than average.

3. Results and discussion

Including the observations presented in this work, optically selected samples of Virgo, Cancer and Coma galaxies (excluding the Hercules supercluster that was only observed as a filler) were nearly completed with Hα imaging observations. Table 3 gives the details. Among 384 Virgo late-type members within the completeness limit of the VCC ($m_{pg} \leq 18.0$), less than two dozen galaxies still need to be observed. In the Coma supercluster (C+G+M+I) only 33 out of 272 galaxies with $m_{pg} \leq 15.7$ still need to be observed. This fraction nearly vanishes among both the cluster members (C) and strictly isolated objects (I).
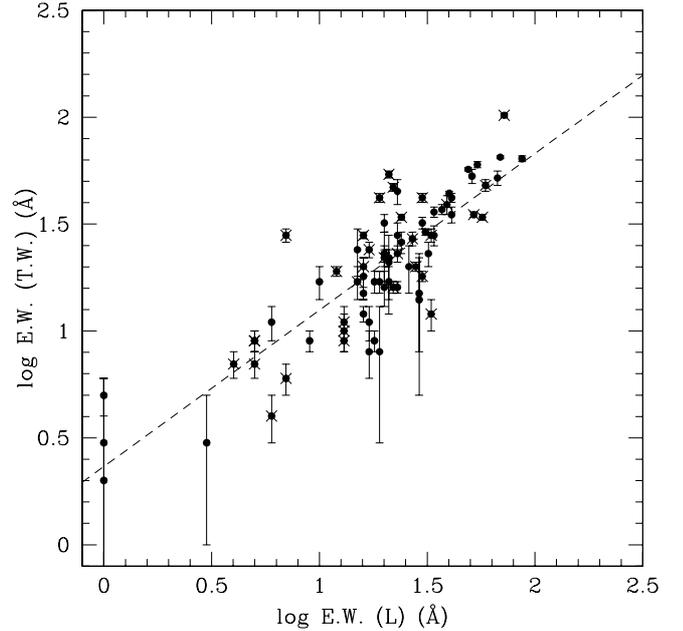

Fig. 3. Comparison of the Hα EW of galaxies measured in this work and those in the literature. The broken line represents the linear regression.
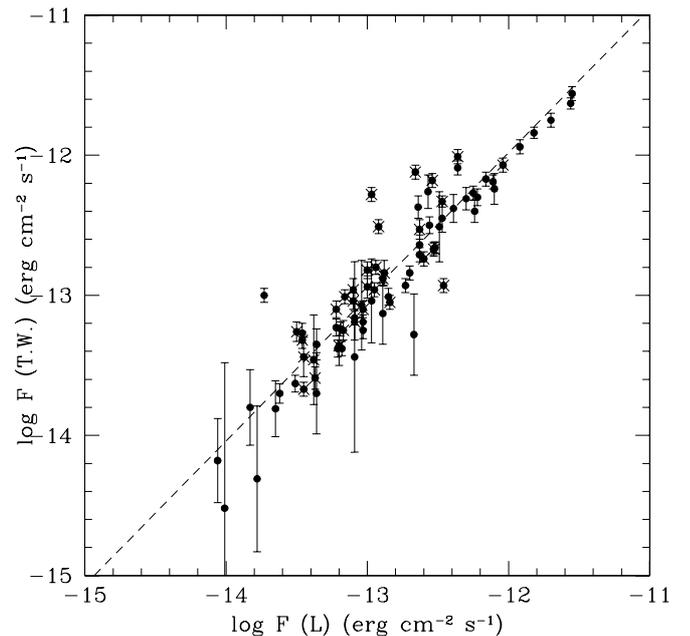

Fig. 4. Comparison of the Hα flux of galaxies measured in this work and those in the literature. The broken line represents the linear regression.

Table 3. Completeness.

	Members	Hα	%
Virgo $m_{pg} \leq 18.0$	384	362	94
Coma+A 1367 (C) $m_{pg} \leq 15.7$	70	67	96
Coma sup. (I) $m_{pg} \leq 15.7$	118	116	98
Coma sup. (G+M+I) $m_{pg} \leq 15.7$	212	172	81
Cancer $m_{pg} \leq 15.7$	35	35	100
Hercules $m_{pg} \leq 15.7$	112	30	27

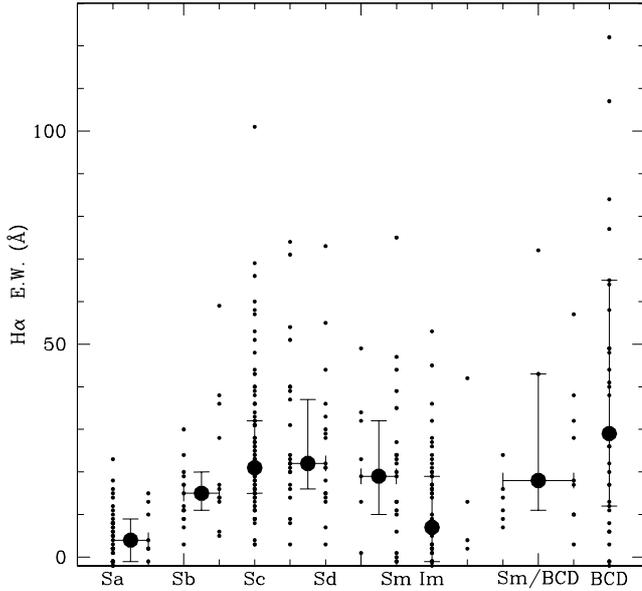**Fig. 5.** Distribution of the individual HαEW measurements in the Virgo cluster along the Hubble sequence (small dots) and of the median HαEW in bins of Hubble type. Error bars are drawn at the 25th and 75th percentile of the distribution.

Fig. 6. Same as Fig. 5, except that filled symbols represent $Def_{HI} \leq 0.4$ (unperturbed) objects and open symbols $Def_{HI} > 0.4$ (HI deficient) galaxies.

3.1. Star-formation rate, Hubble type and HI content

Taking advantage of the accurate morphological classification that was achieved for the Virgo cluster, owing to the superb plate quality of the photographic survey by Binggeli et al. (1985) and to the completeness of the present observations, we wish to comment on the dependence of the star-formation properties of late-type galaxies in this cluster on the Hubble type. Figure 5 shows the distribution of the current massive star-formation rate per unit mass, as represented by the individual HαEW measurements, along the Hubble sequence. Taking medians in bins of Hubble type, it appears that the star-formation rate per unit mass in giant galaxies members of the Virgo cluster increases from Sa ($\langle$HαEW$\rangle$ = 4 Å) to Sb ($\langle$HαEW$\rangle$ = 15 Å), Sc ($\langle$HαEW$\rangle$ = 21 Å) and Scd ($\langle$HαEW$\rangle$ = 22 Å); then it decreases to a relative minimum for Im ($\langle$HαEW$\rangle$ = 7 Å) and reaches the highest value for BCDs ($\langle$HαEW$\rangle$ = 29 Å) (cf. similar results for isolated galaxies in Fig. 3 of Kennicutt 1998). In bins of all types the dispersion of the data exceeds tens of Å, reflecting a dependence of the HαEW on other parameters, within each Hubble class. The main dependency is the one on the galaxy global HI content, as already noted by Boselli et al. (2001) and Gavazzi et al. (2002b). Using the complete compilation of HI deficiency parameters of galaxies in the Virgo cluster by Gavazzi et al. (2005), we show in Fig. 6 the HαEW vs. Hubble type diagram, separately for $Def_{HI} < 0.4$ (unperturbed galaxies) and $Def_{HI} > 0.4$ (HI deficient objects), and in Fig. 7 the distribution of the HαEW in the Virgo cluster in four bins of Hubble type, given separately for $Def_{HI} < 0.4$ and $Def_{HI} > 0.4$. The figures emphasize that, within each Hubble type class, galaxies with normal HI content have HαEW that is systematically higher than their HI deficient counterparts by a factor of two. Moreover, the figures show that the relative minimum found for Im galaxies is not due to a particularly high
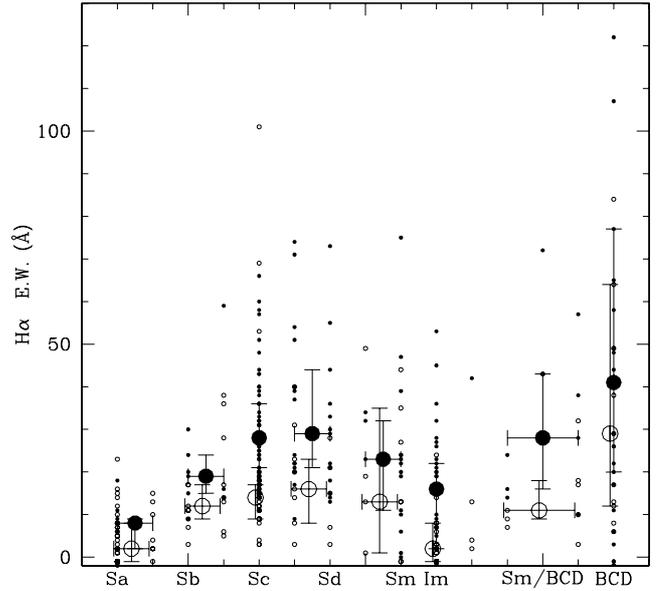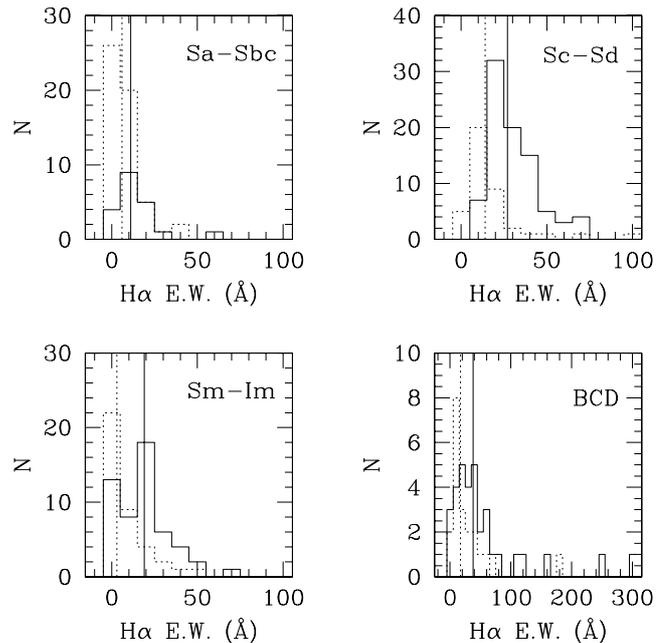

Fig. 7. Distribution of HαEW in the Virgo cluster in four bins of Hubble type, divided in $Def_{HI} \leq 0.4$ (solid histogram) and $Def_{HI} > 0.4$ (dotted histogram). Vertical lines mark the median of each distribution.

HI deficiency among these objects, but is a characteristic of all objects in this Hubble class.

3.2. The radial dependence of the star-formation rate in nearby clusters

One of the hottest issues in galaxy evolution is whether the star-formation rate depends on the environmental properties of galaxies, i.e. on the local galaxy density and/or projected

distances from galaxy density enhancements (clusters). The 2dF (Lewis et al. 2002) and the SDSS surveys (Gomez et al. 2003; Goto 2003; Nichol 2004; Kauffmann et al. 2004) have clearly shown that the star-formation rate is found to be significantly quenched when the galaxy density overcomes the characteristic value of $\sim 1\ h_{75}^{-2}\ \mathrm{Mpc}^{-2}$, i.e. between 1 to 2 virial radii from cluster centers, which is the regime where significant gas depletion occurs (van Gorkom et al. 2004). These works, however, are limited by the lack of a reliable morphological classification for their objects (in fact based on light concentration and/or spectrophotometric indicators), and thus they cannot disentangle the radial dependence of the star-formation activity from the morphology-segregation effect. Furthermore, SDSS and 2dF only include high-luminosity ($M_r \leq -20.5$ for SDSS and $M_B \leq -19$ for 2dF) galaxies that are shallower or similar to our survey of Coma ($M_B \leq -19.2$) and much shallower than Virgo ($M_B \leq -13$).

Gavazzi et al. (2002b), analyzing the Hα properties of spiral galaxies that were available prior to 2003, found indications that only high luminosity objects show the expected decrease of SFR with decreasing projected distance from the center of Virgo, A 1367 and Coma, while low luminosity galaxies show an opposite trend. Taking advantage of the presently complete Hα survey, we re-analyzed the dependence of the HαEW on the clustercentric radius in units of Virial radii, assuming 1.7 Mpc for Virgo and 2.2 Mpc for Coma (Figs. 8 and 9; Girardi et al. 1998). Virgo galaxies are subdivided in high and low luminosity (above and below $B_T^o = -19.0$) according to their Blue luminosity, which is available for the majority of galaxies (see Col. 13 of Table 1). For Coma and A 1367 (combined) we instead used a threshold based on the Near-IR (H band) luminosity available for all galaxies in the Coma supercluster, as it provided the best estimate of the dynamical mass within the galaxies optical extent (Gavazzi et al. 1996). The luminosity threshold ($L_H = 10.5$) adopted for Coma is on average half a magnitude brighter than the one adopted for Virgo. Both distributions did not appear to be strong functions of the clustercentric distance. Low-luminosity galaxies have systematically higher EW than high-luminosity ones and this difference is highest at radii below $1.5R_{\mathrm{vir}}$, reflecting a possible suppression of SFR for giant galaxies. The decline in SFR (as expressed by the HαEW) is clearer for giant late-type galaxies in the Virgo cluster from 2 to 0.5 R_{vir}. On the contrary, we did not identify any significant trend with clustercentric distance for the dwarf spirals.

The different patterns of high and low luminosity could be observed by neither the 2dF nor SDSS surveys due to their shallowness, which indicates that giant spiral galaxies within the virial radius were subject to gas removal long enough for their SFR to be significantly quenched. Dwarf galaxies instead might have had less time to develop such depletion, because rich clusters are being significantly replenished with small galaxies at the present cosmological epoch. Favoring this hypothesis, we found that low and high luminosity late-type members of these three clusters have significantly different velocity distributions, with the distribution of the low luminosity objects broader and more deviating from a Gaussian than that of the high luminosity objects (see Adami et al. 1998). For the Virgo cluster, owing
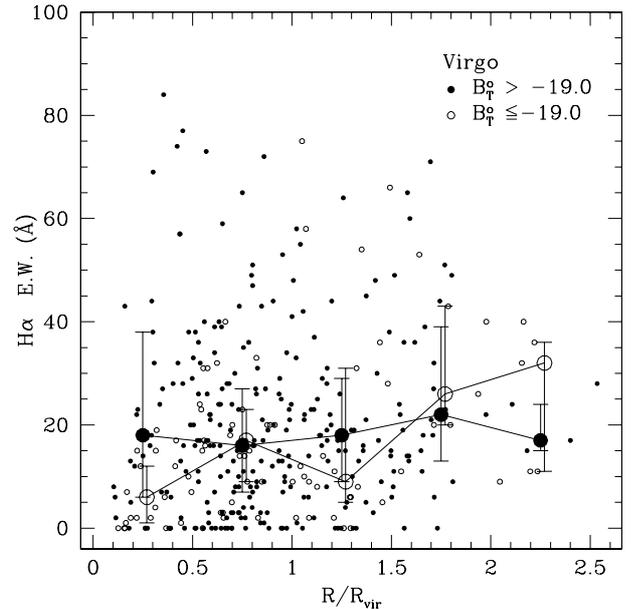

Fig. 8. The clustercentric radial distribution of the individual HαEW measurements in the Virgo cluster. High and low (B-band) luminosity galaxies are given with open and filled dots, respectively. Median in bins of 0.5 R/R_{Vir} are given. Error bars mark the 25th and 75th percentile of the distribution.

to the detailed morphological classification available from the VCC, it is possible to divide up the 729 members with known velocity ($-1000 < V < 3000$ km s^{-1}) between early and late (>Sa) types. Among the latter, the velocity dispersion of the 50 brightest ($m_{\mathrm{pg}} < 12.5$) galaxies is 782 km s^{-1}. Fainter than $m_{\mathrm{pg}} = 12.5, 13.5, 14.5$, it becomes 1570, 1717, 1911 km s^{-1}, respectively.

4. Summary

The Hα flux and equivalent width of 273 galaxies obtained with the SPM 2.1 m and with the ESO/3.6 m telescopes have been presented. These observations conclude the long-term Hα survey of late-type galaxies in the Virgo, Coma, A 1367 and Cancer clusters, as well as of relatively isolated objects in the Great Wall, spanning a wide range of morphological type, luminosity and environmental conditions.

In the Virgo cluster in particular, all giant spirals and virtually all late-type dwarfs were observed down to the optical limit of $m_{\mathrm{pg}} = 18$ mag ($M_{\mathrm{pg}} = -13$ mag).

From these data we conclude that:

1) The star-formation rate per unit mass in giant galaxy members of the Virgo cluster increases from Sa to Scd, then decreases to a relative minimum for Im, finally reaching the highest peak for BCDs.
2) Within each Hubble type class, galaxies with normal HI content have twice the HαEW of their HI-deficient counterparts.
3) The SFR per unit mass of high luminosity spirals that are projected within 1 virial radius is about a factor of two lower than at larger clustercentric projected distances. Low
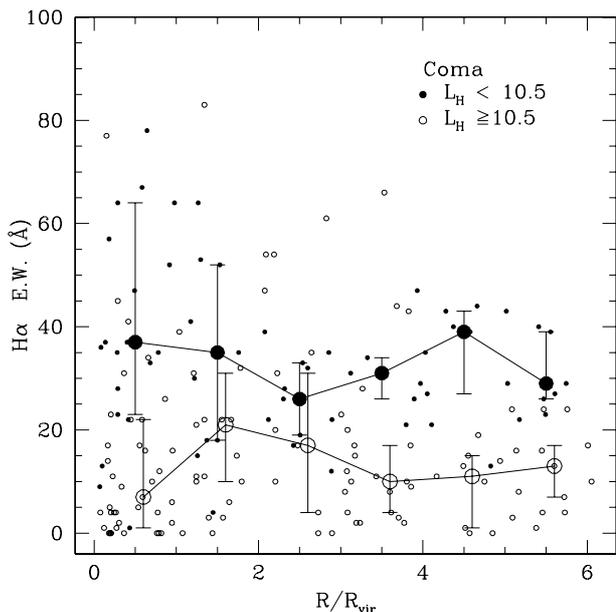
Fig. 9. The clustercentric radial distribution of the individual Hα*EW* measurements in the Coma+A 1367 clusters and in the Great Wall. High and low (*H*-band) luminosity galaxies are given with open and filled dots, respectively. The median in bins of 1 $R/R_{\rm Vir}$ are given. Error bars mark the 25th and 75th percentile of the distribution.

luminosity objects have similar Hα properties at all cluster-centric radii.

Analysis of the full Hα data-set, including study of the galacto-centric radial distribution of the star-forming regions as a function of other environmental indicators (i.e. gaseous properties of galaxies in and outside rich clusters) will be presented in a forthcoming paper of this series (Paper VI: The morphology of the star-forming regions, in preparation).

References

Adami, C., Biviano, A., & Mazure, A. 1998, A&A, 331, 439
Almoznino, E., & Brosch, N. 1998, MNRAS, 298, 931
Binggeli, B., Sandage, A., & Tammann, G. 1985, AJ, 90, 1681 (VCC)
Binggeli, B., Popescu, C., & Tammann, G. 1993, A&AS, 98, 275
Boselli, A., Gavazzi, G., Donas, J., & Scodeggio, M. 2001, AJ, 121, 753
Boselli, A., & Gavazzi, G. 2002, A&A, 386, 124 (Paper II)
Boselli, A., Iglesias-Paramo, J., Vilchez, J., & Gavazzi, G. 2002, A&A, 386, 134 (Paper III)
Boselli, A., Gavazzi, G., & Sanvito, G. 2003, A&A, 402, 37
Bothun, G. D., Geller, M. J., Beers, T. C., & Huchra, J. P. 1983, ApJ, 268, 47
Burstein, D., & Heiles, C. 1978, ApJ, 225, 40
Gallagher, J., & Hunter, D. 1989, AJ, 98, 806
Gavazzi, G., Boselli, A., & Kennicutt, R. 1991, AJ, 101, 1207
Gavazzi, G., & Boselli, A. 1996, Astro. Lett. & Comm., 35, 1
Gavazzi, G., Pierini, D., & Boselli, A. 1996, A&A, 312, 397
Gavazzi, G., Catinella, B., Carrasco, L., Boselli, A., & Contursi, A. 1998, AJ, 115, 1745
Gavazzi, G., Boselli, A., Pedotti, P., Gallazzi, A., & Carrasco, L. 2002a, A&A, 386, 114 (Paper I)
Gavazzi, G., Boselli, A., Pedotti, P., Gallazzi, A., & Carrasco, L. 2002b, A&A, 396, 449 (Paper IV)
Gavazzi, G., Boselli, A., Scodeggio, M., Pierini, D., & Belsole, E. 1999a, MNRAS, 304, 595
Gavazzi, G., Carrasco, L., & Galli, R. 1999b, A&AS, 136, 227
Gavazzi, G., Boselli, A., Donati, A., Franzetti, P., & Scodeggio, M. 2003, A&A, 400, 451
Gavazzi, G., Boselli, A., van Driel, W., & O'Neil, K. 2005, A&A, 429, 439
Girardi, M., Giuricin, G., Mardirossian, F., Mezzetti, M., & Boschin, W. 1998, ApJ, 505, 74
Gomez, P. L., Nichol, R. C., & Miller, C. J. 2003, ApJ, 584, 210
Goto, T., Okamura, S., & Sekiguchi, M. 2003, PASJ, 55, 757
Haynes, M. P., & Giovanelli, R. 1984, AJ, 89, 758
Hamuy, M., Suntzeff, N. B., Heathcote, S. R., et al. 1994, PASP, 106, 566
Heller, A., Almoznino, E., & Brosch, N. 1999, MNRAS, 304, 8
Iglesias-Paramo, J., Boselli, A., Cortese, L., Vilchez, J., & Gavazzi, G. 2002, A&A, 384, 383
James, P. A., Shane, N. S., Beckman, J. E., et al. 2004, A&A, 414, 23
Kauffmann, G., et al. 2004, MNRAS, 353, 713
Kennicutt, R. 1998, ARA&A, 36, 189
Kennicutt, R., & Kent, S. 1983, AJ, 88, 1094
Kennicutt, R., Bothun, G., & Schommer, R. 1984, AJ, 89, 1279
Koopmann, R., Kenney, J., & Joung, J. 2001, ApJS, 135, 125
Koopmann, R., & Kenney, J. 2004a, ApJ, 613, 851
Koopmann, R., & Kenney, J. 2004b, ApJ, 613, 866
Lewis, I., Balogh, M., De Propris, R., et al. 2002, MNRAS, 334, 673
Massey, P., Strobel, K., Barnes, J., & Anderson, E. 1988, ApJ, 328, 315
Moss, C., Irwin, M. J., & Whittle, M. 1988, MNRAS, 232, 381
Moss, C., Whittle, M., & Pesce, J. E. 1998, MNRAS, 300, 205
Moss, C., & Whittle, M. 2000, MNRAS, 317, 667
Nichol, R. C. 2004, in Clusters of Galaxies: Probes of Cosmological Structure and Galaxy Evolution, from the Carnegie Observatories Centennial Symposia (Cambridge University Press), Carnegie Observatories Astrophysics Series, ed. J. S. Mulchaey, A. Dressler, & A. Oemler, 24
Nilson, P. 1973, Uppsala General Catalogue of Galaxies, Uppsala Obs. Ann., 6 (UGC)
Romanishin, W. 1990, AJ, 100, 373
Sakai, S., Kennicutt, R. C., & Moss, C. 2001, AAS, 198.0703S
Usui, T., Saito, M., & Tomita, A. 1998, AJ, 116, 2166
van Gorkom, J. H. 2004, in Clusters of Galaxies: Probes of Cosmological Structure and Galaxy Evolution, 306
Zwicky, F., Herzog, E., Karpowicz, M., Kowal, C., & Wild, P. 1961–1968, Catalogue of Galaxies and of Cluster of Galaxies, Pasadena, California Institute of Technology, CGCG